A monolithic FEM/Multigrid solver for ALE formulation of fluid structure interaction with application in biomechanics

Jaroslav Hron and Stefan Turek*

Institute for Applied Mathematics and Numerics, University of Dortmund, Vogelpothsweg 87, 44227 Dortmund, Germany

Abstract. We investigate a new method of solving the problem of fluid-structure interaction of an incompressible elastic object in laminar incompressible viscous flow. Our proposed method is based on a fully implicit, monolithic formulation of the problem in the arbitrary Lagrangian-Eulerian framework. High order FEM is used to obtain the discrete approximation of the problem. In order to solve the resulting systems a quasi-Newton method is applied with the linearized systems being approximated by the divided differences approach. The linear problems of saddle-point type are solved by a standard geometric multigrid with local multilevel pressure Schur complement smoothers.

1 Overview

We consider the problem of viscous fluid flow interacting with an elastic body which is being deformed by the fluid action. Such a problem is encountered in many real life applications of great importance. Typical examples of this type of problem are the areas of aero-elasticity, biomechanics or material processing. For example, a good mathematical model for biological tissue could be used in such areas as early recognition or prediction of heart muscle failure, advanced design of new treatments and operative procedures, and the understanding of atherosclerosis and associated problems. Other possible applications include the development of virtual reality programs for training new surgeons or designing new operative procedures (see [12]).

1.1 Fluid structure models in biomechanics

There have been several different approaches to the problem of fluid-structure interaction. Most notably these include the work of [13, 14, 15, 16] where an immersed boundary method was developed and applied to a three-dimensional model of the heart. In this model they consider a set of one-dimensional elastic fibers immersed in a three-dimensional fluid region and using a parallel supercomputer they were able to model the pulse of the heart ventricle.

* This work has been supported by German Reasearch Association (DFG), Reasearch unit 493.

A fluid-structure model with the wall modelled as a thin shell was used to model the left heart ventricle in [3, 4] and [18, 17]. In [7, 8] a similar approach was used to model the flow in a collapsible tube. In these models the wall is modelled by two-dimensional thin shells which can be modified to capture the anisotropy of the muscle. In reality the thickness of the wall can be significant and very important. For example in arteries the wall thickness can be up to 30% of the diameter and its local thickening can lead to the creation of an aneurysm. In the case of heart ventricle the thickness of the wall is also significant and also the direction of the muscle fibers changes through the wall.

1.2 Theoretical results

The theoretical investigation of fluid structure interaction problems is complicated by the need of mixed description. While for the solid part the natural view is the material (Lagrangian) description, for the fluid it is the spatial (Eulerian) description. In the case of their combination some kind of mixed description (usually referred to as the arbitrary Lagrangian-Eulerian description or ALE) has to be used which brings additional nonlinearity into the resulting equations.

In [10] a time dependent, linearized model of interaction between a viscous fluid and an elastic shell in small displacement approximation and its discretization is analyzed. The problem is further simplified by neglecting all changes in the geometry configuration. Under these simplifications by using energy estimates they are able to show that the proposed formulation is well posed and a global weak solution exists. Further they show that an independent discretization by standard mixed finite elements for the fluid and by nonconforming discrete Kirchhoff triangle finite elements for the shell together with backward or central difference approximation of the time derivatives converges to the solution of the continuous problem.

In [19] a steady problem of equilibrium of an elastic fixed obstacle surrounded by a viscous fluid is studied. Existence of an equilibrium state is shown with the displacement and velocity in $C^{2,\alpha}$ and pressure in $C^{1,\alpha}$ under assumption of small data in $C^{2,\alpha}$ and domain boundaries of class C^3.

A numerical solution of the resulting equations of the fluid structure interaction problem poses a great challenge since it includes the features of nonlinear elasticity, fluid mechanics and their coupling. The easiest solution strategy, mostly used in the available software packages, is to decouple the problem into the fluid part and solid part, for each of those parts to use some well established method of solution then the interaction is introduced as external boundary conditions in each of the subproblems. This has an advantage that there are many well tested finite element based numerical methods for separate problems of fluid flow and elastic deformation, on the other hand the treatment of the interface and the interaction is problematic. The approach presented here treats the problem as a single continuum with

the coupling automatically taken care of as internal interface, which in our formulation does not require any special treatment.

2 Continuum description

Let $\Omega \subset \mathbb{R}^3$ be a reference configuration of a given body. Let $\Omega_t \subset \mathbb{R}^3$ be a configuration of this body at time t. Then a one-to-one, sufficiently smooth mapping $\boldsymbol{\chi}_\Omega$ of the reference configuration Ω to the current configuration

$$\boldsymbol{\chi}_\Omega : \Omega \times [0,T] \mapsto \mathbb{R}^3, \tag{1}$$

describes the motion of the body, see figure 1. The mapping $\boldsymbol{\chi}_\Omega$ depends on the choice of the reference configuration Ω which can be fixed in a various ways. Here we think of Ω to be the initial (stress-free) configuration Ω_0. Thus, if not emphasized, we mean by $\boldsymbol{\chi}$ exactly $\boldsymbol{\chi}_\Omega = \boldsymbol{\chi}_{\Omega_0}$.

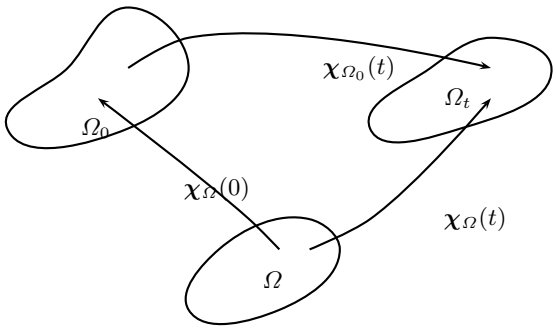

Fig. 1. The referential domain Ω, initial Ω_0 and current state Ω_t and relations between them. The identification $\Omega \equiv \Omega_0$ is adopted in this text.

If we denote by $\boldsymbol{X}$ a material point in the reference configuration Ω then the position of this point at time t is given by

$$\boldsymbol{x} = \boldsymbol{\chi}(\boldsymbol{X}, t). \tag{2}$$

Next, the mechanical fields describing the deformation are defined in a standard manner. The displacement field, the velocity field, deformation gradient and its determinant are

$$\boldsymbol{u}(\boldsymbol{X},t) = \boldsymbol{\chi}(\boldsymbol{X},t) - \boldsymbol{X}, \qquad \boldsymbol{v} = \frac{\partial \boldsymbol{\chi}}{\partial t}, \qquad \boldsymbol{F} = \frac{\partial \boldsymbol{\chi}}{\partial \boldsymbol{X}}, \qquad J = \det \boldsymbol{F}. \tag{3}$$

Let us adopt the following useful notations for some derivatives. Any field quantity φ with values in some vector space Y (i.e. scalar, vector or tensor valued) can be expressed in the Eulerian description as a function of the spatial position $\boldsymbol{x} \in \mathbb{R}^3$

$$\varphi = \tilde{\varphi}(\boldsymbol{x}, t) : \Omega_t \times [0,T] \mapsto Y.$$

Then we define following notations for the derivatives of the field φ

$$\frac{\partial \varphi}{\partial t} := \frac{\partial \tilde{\varphi}}{\partial t}, \qquad \nabla \varphi = \frac{\partial \varphi}{\partial \boldsymbol{x}} := \frac{\partial \tilde{\varphi}}{\partial \boldsymbol{x}}, \qquad \operatorname{div} \varphi := \operatorname{tr} \nabla \varphi. \tag{4}$$

In the case of Lagrangian description we consider the quantity φ to be defined on the reference configuration Ω, then for any $\boldsymbol{X} \in \Omega$ we can express the quantity φ as

$$\varphi = \bar{\varphi}(\boldsymbol{X}, t) : \Omega \times [0, T] \mapsto Y,$$

and we define the derivatives of the field φ as

$$\frac{d \varphi}{dt} := \frac{\partial \bar{\varphi}}{\partial t}, \qquad \operatorname{Grad} \varphi = \frac{\partial \varphi}{\partial \boldsymbol{X}} := \frac{\partial \bar{\varphi}}{\partial \boldsymbol{X}}, \qquad \operatorname{Div} \varphi := \operatorname{tr} \operatorname{Grad} \varphi. \tag{5}$$

These two descriptions can be related to each other through following relations

$$\bar{\varphi}(\boldsymbol{X}, t) = \tilde{\varphi}(\boldsymbol{\chi}(\boldsymbol{X}, t), t), \tag{6}$$

$$\frac{d \varphi}{dt} = \frac{\partial \varphi}{\partial t} + (\nabla \varphi) \boldsymbol{v}, \qquad \operatorname{Grad} \varphi = (\nabla \varphi) \boldsymbol{F}, \qquad \int_{\Omega_t} \varphi dv = \int_{\Omega} \varphi J dV \tag{7}$$

$$\frac{d \boldsymbol{F}}{dt} = \operatorname{Grad} \boldsymbol{v}, \qquad \frac{\partial J}{\partial \boldsymbol{F}} = J \boldsymbol{F}^{-T}, \qquad \frac{dJ}{dt} = J \operatorname{div} \boldsymbol{v}. \tag{8}$$

For the formulation of the balance laws we will need to express a time derivatives of some integrals. The following series of equalities obtained by using the previously stated relations will be useful

$$\begin{aligned} \frac{d}{dt} \int_{\Omega_t} \varphi dv &= \frac{d}{dt} \int_{\Omega} \varphi J dV = \int_{\Omega} \frac{d}{dt} (\varphi J) \, dV = \int_{\Omega_t} \left(\frac{d \varphi}{dt} + \varphi \operatorname{div} \boldsymbol{v} \right) dv \\ &= \int_{\Omega_t} \left(\frac{\partial \varphi}{\partial t} + \operatorname{div} (\varphi \boldsymbol{v}) \right) dv = \int_{\Omega_t} \frac{\partial \varphi}{\partial t} dv + \int_{\partial \Omega_t} \varphi \boldsymbol{v} \cdot \boldsymbol{n} da \\ &= \frac{\partial}{\partial t} \int_{\Omega_t} \varphi dv + \int_{\partial \Omega_t} \varphi \boldsymbol{v} \cdot \boldsymbol{n} da. \end{aligned} \tag{9}$$

And also the Piola identity will be used, $\operatorname{Div}(J \boldsymbol{F}^{-T}) = \boldsymbol{0}$, which can be checked by differentiating the left hand side and using (8) together with an identity obtained by differentiating the relation $\boldsymbol{F} \boldsymbol{F}^{-1} = \boldsymbol{I}$.

2.1 Balance laws

In this section we will formulate the balance relations for mass and momentum in three forms: the Eulerian, the Lagrangian and the arbitrary Eulerian-Lagrangian (ALE) description.

The Eulerian (or spatial) description is well suited for a problem of fluid flowing through some spatially fixed region. In such a case the material particles can enter and leave the region of interest. The fundamental quantity describing the motion is the velocity vector.

On the other hand the Lagrangian (or referential) description is well suited for a problem of deforming a given body consisting of a fixed set of material particles. In this case the actual boundary of the body can change its shape. The fundamental quantity describing the motion in this case is the vector of displacement from the referential state.

In the case of fluid-structure interaction problems we can still use the Lagrangian description for the deformation of the solid part. The fluid flow now takes place in a domain with boundary given by the deformation of the structure which can change in time and is influenced back by the fluid flow. The mixed ALE description of the fluid has to be used in this case. The fundamental quantity describing the motion of the fluid is still the velocity vector but the description is accompanied by a certain displacement field which describes the change of the fluid domain. This displacement field has no connection to the fluid velocity field and the purpose of its introduction is to provide a transformation of the current fluid domain and corresponding governing equations to some fixed reference domain. This method is sometimes called a pseudo-solid mapping method [see 20].

Let $\mathcal{P} \subset \mathbb{R}^3$ be a fixed region in space (a control volume) with the boundary $\partial\mathcal{P}$ and unit outward normal vector $\boldsymbol{n}_{\mathcal{P}}$, such that

$$\mathcal{P} \subset \Omega_t \quad \text{for all } t \in [0,T].$$

Let ϱ denote the mass density of the material. Then the balance of mass in the region $\mathcal{P}$ can be written as

$$\frac{\partial}{\partial t}\int_{\mathcal{P}} \varrho dv + \int_{\partial\mathcal{P}} \varrho \boldsymbol{v}\cdot\boldsymbol{n}_{\mathcal{P}} da = 0. \tag{10}$$

If all the fields are sufficiently smooth this equation can be written in local form with respect to the current configuration as

$$\frac{\partial \varrho}{\partial t} + \operatorname{div}(\varrho \boldsymbol{v}) = 0. \tag{11}$$

It will be useful to derive the mass balance equation from the Lagrangian point of view. Let $\mathcal{Q} \subset \Omega$ be a fixed set of particles. Then $\boldsymbol{\chi}(\mathcal{Q},t) \subset \Omega_t$ is a region occupied by these particles at the time t, and the balance of mass can be expressed as

$$\frac{d}{dt}\int_{\boldsymbol{\chi}(\mathcal{Q},t)} \varrho dv = 0, \tag{12}$$

which in local form w.r.t. the reference configuration can be written as

$$\frac{d}{dt}(\varrho J) = 0. \tag{13}$$

In the case of an arbitrary Lagrangian-Eulerian description we take a region $\mathcal{Z} \subset \mathbb{R}^3$ which is itself moving independently of the motion of the body. Let the motion of the control region $\mathcal{Z}$ be described by a given mapping

$$\boldsymbol{\zeta}_{\mathcal{Z}} : \mathcal{Z} \times [0,T] \mapsto \mathbb{R}^3, \qquad \mathcal{Z}_t \subset \Omega_t \quad \forall t \in [0,T],$$

with the corresponding velocity $\boldsymbol{v}_{\mathcal{Z}} = \frac{\partial \boldsymbol{\zeta}_{\mathcal{Z}}}{\partial t}$, deformation gradient $\boldsymbol{F}_{\mathcal{Z}} = \frac{\partial \boldsymbol{\zeta}_{\mathcal{Z}}}{\partial \boldsymbol{X}}$ and its determinant $J_{\mathcal{Z}} = \det \boldsymbol{F}_{\mathcal{Z}}$. The mass balance equation can be written as

$$\frac{\partial}{\partial t} \int_{\mathcal{Z}_t} \varrho dv + \int_{\partial \mathcal{Z}_t} \varrho (\boldsymbol{v} - \boldsymbol{v}_{\mathcal{Z}}) \cdot \boldsymbol{n}_{\mathcal{Z}_t} da = 0, \tag{14}$$

this can be viewed as an Eulerian description with a moving spatial coordinate system or as a grid deformation in the context of the finite element method. In order to obtain a local form of the balance relation we need to transform the integration to the fixed spatial region $\mathcal{Z}$

$$\frac{\partial}{\partial t} \int_{\mathcal{Z}} \varrho J_{\mathcal{Z}} dv + \int_{\partial \mathcal{Z}} \varrho (\boldsymbol{v} - \boldsymbol{v}_{\mathcal{Z}}) \cdot \boldsymbol{F}_{\mathcal{Z}}^{-T} \boldsymbol{n}_{\mathcal{Z}} J_{\mathcal{Z}} da = 0, \tag{15}$$

then the local form is

$$\frac{\partial}{\partial t} (\varrho J_{\mathcal{Z}}) + \operatorname{div} \left(\varrho J_{\mathcal{Z}} (\boldsymbol{v} - \boldsymbol{v}_{\mathcal{Z}}) \cdot \boldsymbol{F}_{\mathcal{Z}}^{-T} \right) = 0. \tag{16}$$

The two previous special formulations can be now recovered. If the region $\mathcal{Z}$ is not moving in space, i.e. $\mathcal{Z} = \mathcal{Z}_t, \forall t \in [0,T]$, then $\boldsymbol{\zeta}_{\mathcal{Z}}$ is the identity mapping, $\boldsymbol{F}_{\mathcal{Z}} = \boldsymbol{I}, J_{\mathcal{Z}} = 1, \boldsymbol{v}_{\mathcal{Z}} = \boldsymbol{0}$ and (16) reduces to (11). If the region $\mathcal{Z}$ moves exactly with the material, i.e. $\boldsymbol{\zeta}_{\mathcal{Z}} = \boldsymbol{\chi}|_{\mathcal{Z}}$ then $\boldsymbol{F}_{\mathcal{Z}} = \boldsymbol{F}, J_{\mathcal{Z}} = J, \boldsymbol{v}_{\mathcal{Z}} = \boldsymbol{v}$ and (16) reduces to (13).

The balance of linear momentum is postulated in a similar way. Let $\boldsymbol{\sigma}$ denote the Cauchy stress tensor field, representing the surface forces per unit area, $\boldsymbol{f}$ be the body forces acting on the material per unit mass. Then the balance of linear momentum in the Eulerian description is stated as

$$\frac{\partial \varrho \boldsymbol{v}}{\partial t} + \operatorname{div}(\varrho \boldsymbol{v} \otimes \boldsymbol{v}) = \operatorname{div} \boldsymbol{\sigma}^T + \varrho \boldsymbol{f}, \tag{17}$$

or with the use of (11) we can write

$$\varrho \frac{\partial \boldsymbol{v}}{\partial t} + \varrho (\nabla \boldsymbol{v}) \boldsymbol{v} = \operatorname{div} \boldsymbol{\sigma}^T + \varrho \boldsymbol{f}. \tag{18}$$

From the Lagrangian point of view the momentum balance relation is

$$\frac{d}{dt} (\varrho J \boldsymbol{v}) = \operatorname{Div} \left(J \boldsymbol{\sigma}^T \boldsymbol{F}^{-T} \right) + \varrho J \boldsymbol{f}, \tag{19}$$

or using (13) we can write

$$\varrho J \frac{d\boldsymbol{v}}{dt} = \mathrm{Div}\left(J\boldsymbol{\sigma}^T \boldsymbol{F}^{-T}\right) + \varrho J \boldsymbol{f}. \tag{20}$$

In the arbitrary Lagrangian-Eulerian formulation we obtain in the local form

$$\frac{\partial \varrho J_{\mathcal{Z}} \boldsymbol{v}}{\partial t} + \mathrm{div}\left(\varrho J_{\mathcal{Z}} \boldsymbol{v} \otimes (\boldsymbol{v} - \boldsymbol{v}_{\mathcal{Z}}) \boldsymbol{F}_{\mathcal{Z}}^{-T}\right) = \mathrm{div}\left(J_{\mathcal{Z}} \boldsymbol{\sigma}^T \boldsymbol{F}_{\mathcal{Z}}^{-T}\right) + \varrho J_{\mathcal{Z}} \boldsymbol{f}, \tag{21}$$

or with the use of (16) we can write

$$\varrho J_{\mathcal{Z}} \frac{\partial \boldsymbol{v}}{\partial t} + \varrho J_{\mathcal{Z}} (\nabla \boldsymbol{v}) \boldsymbol{F}_{\mathcal{Z}}^{-T} (\boldsymbol{v} - \boldsymbol{v}_{\mathcal{Z}}) = \mathrm{div}\left(J_{\mathcal{Z}} \boldsymbol{\sigma}^T \boldsymbol{F}_{\mathcal{Z}}^{-T}\right) + \varrho J_{\mathcal{Z}} \boldsymbol{f}. \tag{22}$$

In the case of angular momentum balance we assume that there are no external or internal sources of angular momentum. It then follows that the Cauchy stress tensor has to be symmetric, i.e. $\boldsymbol{\sigma} = \boldsymbol{\sigma}^T$. Assuming isothermal conditions the energy balance is satisfied if the choice of the constitutive relation for the materials is compatible with the balance of entropy.

3 Fluid structure interaction problem formulation

At this point we make a few assumptions that allow us to deal with the task of setting up a tractable problem. Let us consider a flow between thick elastic walls as shown in figure 2. We will use the superscripts ^{s} and ^{f} to denote the quantities connected with the solid and fluid. Let us assume that both materials are incompressible and all the processes are isothermal, which is a well accepted approximation in biomechanics, and let us denote the constant densities of each material by ϱ^f, ϱ^s.

3.1 Monolithic description

We denote by Ω_t^f the domain occupied by the fluid and Ω_t^s by the solid at time $t \in [0, T]$. Let $\Gamma_t^0 = \bar{\Omega}_t^f \cap \bar{\Omega}_t^s$ be the part of the boundary where the solid interacts with the fluid and $\Gamma_t^i, i = 1, 2, 3$ be the remaining external boundaries of the solid and the fluid as depicted in figure 2.

Let the deformation of the solid part be described by the mapping $\boldsymbol{\chi}^s$

$$\boldsymbol{\chi}^s : \Omega^s \times [0, T] \mapsto \mathbb{R}^3, \tag{23}$$

with the corresponding displacement $\boldsymbol{u}^s$ and the velocity $\boldsymbol{v}^s$ given by

$$\boldsymbol{u}^s(\boldsymbol{X}, t) = \boldsymbol{\chi}^s(\boldsymbol{X}, t) - \boldsymbol{X}, \qquad \boldsymbol{v}^s(\boldsymbol{X}, t) = \frac{\partial \boldsymbol{\chi}^s}{\partial t}(\boldsymbol{X}, t). \tag{24}$$

The fluid flow is described by the velocity field $\boldsymbol{v}^f$ defined on the fluid domain Ω_t^f

$$\boldsymbol{v}^f(\boldsymbol{x}, t) : \Omega_t^f \times [0, T] \mapsto \mathbb{R}^3. \tag{25}$$

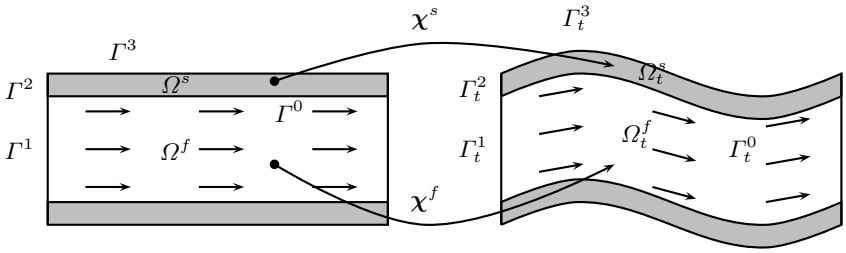

Fig. 2. Undeformed (original) and deformed (current) configurations.

Further we define the auxiliary mapping, denoted by $\boldsymbol{\zeta}^f$, to describe the change of the fluid domain and corresponding displacement $\boldsymbol{u}^f$ by

$$\boldsymbol{\zeta}^f : \Omega^f \times [0,T] \mapsto \mathbb{R}^3, \qquad \boldsymbol{u}^f(\boldsymbol{X},t) = \boldsymbol{\zeta}^f(\boldsymbol{X},t) - \boldsymbol{X}. \tag{26}$$

We require that the mapping $\boldsymbol{\zeta}^f$ is sufficiently smooth, one to one and has to satisfy

$$\boldsymbol{\zeta}^f(\boldsymbol{X},t) = \boldsymbol{\chi}^s(\boldsymbol{X},t), \quad \forall (\boldsymbol{X},t) \in \Gamma^0 \times [0,T]. \tag{27}$$

In the context of the finite element method this will describe the artificial mesh deformation inside the fluid region and it will be constructed as a solution to a suitable boundary value problem with (27) as the boundary condition.

The momentum and mass balance of the fluid in the time dependent fluid domain according to (16) and (21) are

$$\varrho^f \frac{\partial \boldsymbol{v}^f}{\partial t} + \varrho^f (\nabla \boldsymbol{v}^f)(\boldsymbol{v}^f - \frac{\partial \boldsymbol{u}^f}{\partial t}) = \operatorname{div} \boldsymbol{\sigma}^f \qquad \text{in } \Omega_t^f, \tag{28}$$

$$\operatorname{div} \boldsymbol{v}^f = 0 \qquad \text{in } \Omega_t^f, \tag{29}$$

together with the momentum (17) and mass (11) balance of the solid in the solid domain

$$\varrho^s \frac{\partial \boldsymbol{v}^s}{\partial t} + \varrho^s (\nabla \boldsymbol{v}^s)\boldsymbol{v}^s = \operatorname{div} \boldsymbol{\sigma}^s \qquad \text{in } \Omega_t^s, \tag{30}$$

$$\operatorname{div} \boldsymbol{v}^s = 0 \qquad \text{in } \Omega_t^s. \tag{31}$$

The interaction is due to the exchange of momentum through the common part of the boundary Γ_t^0. On this part we require that the forces are in balance and simultaneously the no slip boundary condition holds for the fluid, i.e.

$$\boldsymbol{\sigma}^f \boldsymbol{n} = \boldsymbol{\sigma}^s \boldsymbol{n} \quad \text{ on } \Gamma_t^0, \qquad \boldsymbol{v}^f = \boldsymbol{v}^s \quad \text{ on } \Gamma_t^0. \tag{32}$$

The remaining external boundary conditions can be of the following kind. A natural boundary condition on the fluid inflow and outflow part Γ_t^1

$$\boldsymbol{\sigma}^f \boldsymbol{n} = p_B \boldsymbol{n} \text{ on } \Gamma_t^1, \tag{33}$$

with p_B given value. Alternatively we can prescribe a Dirichlet type boundary condition on the inflow or outflow part Γ_t^1

$$\boldsymbol{v}^f = \boldsymbol{v}_B \text{ on } \Gamma_t^1, \tag{34}$$

where $\boldsymbol{v}_B$ is given. The Dirichlet boundary condition is prescribed for the solid displacement at the part Γ_t^2

$$\boldsymbol{u}^s = \boldsymbol{0} \text{ on } \Gamma_t^2, \tag{35}$$

and the stress free boundary condition for the solid is applied at the part Γ_t^3

$$\boldsymbol{\sigma}^s \boldsymbol{n} = \boldsymbol{0} \text{ on } \Gamma_t^3. \tag{36}$$

We introduce the domain $\Omega = \Omega^f \cup \Omega^s$, where Ω^f, Ω^s are the domains occupied by the fluid and solid in the initial undeformed state, and two fields defined on this domain as

$$\boldsymbol{u} : \Omega \times [0,T] \to \mathbb{R}^3, \qquad \boldsymbol{v} : \Omega \times [0,T] \to \mathbb{R}^3,$$

such that the field $\boldsymbol{v}$ represents the velocity at the given point and $\boldsymbol{u}$ the displacement on the solid part and the artificial displacement in the fluid part, taking care of the fact that the fluid domain is changing with time,

$$\boldsymbol{v} = \begin{cases} \boldsymbol{v}^s & \text{on } \Omega^s, \\ \boldsymbol{v}^f & \text{on } \Omega^f, \end{cases} \qquad \boldsymbol{u} = \begin{cases} \boldsymbol{u}^s & \text{on } \Omega^s, \\ \boldsymbol{u}^f & \text{on } \Omega^f. \end{cases} \tag{37}$$

Due to the conditions (27) and (32) both fields are continuous across the interface Γ_t^0 and we can define global quantities on Ω as the deformation gradient and its determinant

$$\boldsymbol{F} = \boldsymbol{I} + \operatorname{Grad} \boldsymbol{u}, \qquad J = \det \boldsymbol{F}. \tag{38}$$

Using this notation the solid balance laws (30) and (31) can be expressed in the Lagrangian formulation with the initial configuration Ω^s as reference, cf. (19),

$$J\varrho^s \frac{d\boldsymbol{v}}{dt} = \operatorname{Div} \boldsymbol{P}^s \qquad \text{in } \Omega^s, \tag{39}$$

$$J = 1 \qquad \text{in } \Omega^s. \tag{40}$$

The fluid equations (28) and (29) are already expressed in the arbitrary Lagrangian-Eulerian formulation with respect to the time dependent region

Ω_t^f, now we transform the equations to the fixed initial region Ω^f by the mapping ζ^f defined by (26)

$$\varrho^f \frac{\partial \boldsymbol{v}}{\partial t} + \varrho^f (\operatorname{Grad} \boldsymbol{v}) \boldsymbol{F}^{-1} (\boldsymbol{v} - \frac{\partial \boldsymbol{u}}{\partial t}) = J^{-1} \operatorname{Div}(J \boldsymbol{\sigma}^f F^{-T}) \qquad \text{in } \Omega^f, \tag{41}$$

$$\operatorname{Div}(J \boldsymbol{v} \boldsymbol{F}^{-T}) = 0 \qquad \text{in } \Omega^f. \tag{42}$$

It remains to prescribe some relation for the mapping ζ^f. In terms of the corresponding displacement $\boldsymbol{u}^f$ we formulate some simple relation together with the Dirichlet boundary conditions required by (27), for example

$$\frac{\partial \boldsymbol{u}}{\partial t} = \Delta \boldsymbol{u} \quad \text{in } \Omega^f, \qquad \boldsymbol{u} = \boldsymbol{u}^s \quad \text{on } \Gamma^0, \qquad \boldsymbol{u} = \boldsymbol{0} \quad \text{on } \Gamma^1. \tag{43}$$

Other choices are possible. For example, the mapping $\boldsymbol{u}^f$ can be realized as a solution of the elasticity problem with the same Dirichlet boundary conditions [see 20].

The complete set of the equations can be written as

$$\frac{\partial \boldsymbol{u}}{\partial t} = \begin{cases} \boldsymbol{v} & \text{in } \Omega^s, \\ \Delta \boldsymbol{u} & \text{in } \Omega^f, \end{cases} \tag{44}$$

$$\frac{\partial \boldsymbol{v}}{\partial t} = \begin{cases} \frac{1}{J\varrho^s} \operatorname{Div} \boldsymbol{P}^s & \text{in } \Omega^s, \\ -(\operatorname{Grad} \boldsymbol{v}) \boldsymbol{F}^{-1} (\boldsymbol{v} - \frac{\partial \boldsymbol{u}}{\partial t}) + \frac{1}{J\varrho^f} \operatorname{Div}(J \boldsymbol{\sigma}^f \boldsymbol{F}^{-T}) & \text{in } \Omega^f, \end{cases} \tag{45}$$

$$0 = \begin{cases} J - 1 & \text{in } \Omega^s, \\ \operatorname{Div}(J \boldsymbol{v} \boldsymbol{F}^{-T}) & \text{in } \Omega^f, \end{cases} \tag{46}$$

with the initial conditions

$$\boldsymbol{u}(0) = \boldsymbol{0} \quad \text{in } \Omega, \qquad \boldsymbol{v}(0) = \boldsymbol{v}_0 \quad \text{in } \Omega, \tag{47}$$

and boundary conditions

$$\boldsymbol{u} = \boldsymbol{0}, \quad \boldsymbol{v} = \boldsymbol{v}_B \quad \text{on } \Gamma^1, \quad \boldsymbol{u} = \boldsymbol{0} \quad \text{on } \Gamma^2, \quad \boldsymbol{\sigma}^s \boldsymbol{n} = \boldsymbol{0} \quad \text{on } \Gamma^3. \tag{48}$$

3.2 Constitutive equations

In order to solve the balance equations we need to specify the constitutive relations for the stress tensors. For the fluid we use the incompressible Newtonian relation

$$\boldsymbol{\sigma}^f = -p^f \boldsymbol{I} + \mu(\nabla \boldsymbol{v}^f + (\nabla \boldsymbol{v}^f)^T), \tag{49}$$

where μ represents the viscosity of the fluid and p^f is the Lagrange multiplier corresponding to the incompressibility constraint (29).

For the solid part we assume that it can be described by an incompressible hyper-elastic material. We specify the Helmholtz potential Ψ and the solid stress is given by

$$\boldsymbol{\sigma}^s = -p^s \boldsymbol{I} + \varrho^s \frac{\partial \Psi}{\partial \boldsymbol{F}} \boldsymbol{F}^T, \tag{50}$$

the first Piola-Kirchhoff stress tensor is then given by

$$\boldsymbol{P}^s = -J p^s \boldsymbol{F}^{-T} + J \varrho^s \frac{\partial \Psi}{\partial \boldsymbol{F}}, \tag{51}$$

where p^s is the Lagrange multiplier corresponding to the incompressibility constraint (40).

Then the material is specified by prescribing the Helmholtz potential as a function of the deformation

$$\Psi = \hat{\Psi}(\boldsymbol{F}) = \tilde{\Psi}(\boldsymbol{C}), \tag{52}$$

where $\boldsymbol{C} = \boldsymbol{F}^T \boldsymbol{F}$ is the right Cauchy-Green deformation tensor. Typical examples for the Helmholtz potential used for isotropic materials like rubber is the Mooney-Rivlin material

$$\tilde{\Psi} = c_1(I_C - 3) + c_2(II_C - 3), \tag{53}$$

where $I_C = \operatorname{tr} \boldsymbol{C}, II_C = \operatorname{tr} \boldsymbol{C}^2 - \operatorname{tr}^2 \boldsymbol{C}, III_C = \det \boldsymbol{C}$ are the invariants of the right Cauchy-Green deformation tensor $\boldsymbol{C}$ and c_i are some material constants. A special case of neo-Hookean material is obtained for $c_2 = 0$. With a suitable choice of the material parameters the entropy inequality and the balance of energy are automatically satisfied.

3.3 Weak formulation

We non-dimensionalize all the quantities by a given characteristic length L and speed V as follows

$$\hat{t} = t\frac{V}{L}, \qquad \hat{\boldsymbol{x}} = \frac{\boldsymbol{x}}{L}, \qquad \hat{\boldsymbol{u}} = \frac{\boldsymbol{u}}{L}, \qquad \hat{\boldsymbol{v}} = \frac{\boldsymbol{v}}{V},$$
$$\hat{\boldsymbol{\sigma}}^s = \boldsymbol{\sigma}^s \frac{L}{\varrho^f V^2}, \qquad \hat{\boldsymbol{\sigma}}^f = \boldsymbol{\sigma}^f \frac{L}{\varrho^f V^2}, \qquad \hat{\mu} = \frac{\mu}{\varrho^f V L}, \qquad \hat{\Psi} = \Psi \frac{L}{\varrho^f V^2},$$

further using the same symbols, without the hat, for the non-dimensional quantities. The non-dimensionalized system with the choice of material rela-

tions, (49) for viscous fluid and (51) for the hyper-elastic solid is

$$\frac{\partial \boldsymbol{u}}{\partial t} = \begin{cases} \boldsymbol{v} & \text{in } \Omega^s, \\ \Delta \boldsymbol{u} & \text{in } \Omega^f, \end{cases} \tag{54}$$

$$\frac{\partial \boldsymbol{v}}{\partial t} = \begin{cases} \frac{1}{\beta} \operatorname{Div}\left(-Jp^s \boldsymbol{F}^{-T} + \frac{\partial \Psi}{\partial \boldsymbol{F}}\right) & \text{in } \Omega^s, \\ -(\operatorname{Grad} \boldsymbol{v})\boldsymbol{F}^{-1}(\boldsymbol{v} - \dfrac{\partial \boldsymbol{u}}{\partial t}) & \\ \quad + \operatorname{Div}\left(-Jp^f \boldsymbol{F}^{-T} + J\mu \operatorname{Grad} \boldsymbol{v}\boldsymbol{F}^{-1}\boldsymbol{F}^{-T}\right) & \text{in } \Omega^f, \end{cases} \tag{55}$$

$$0 = \begin{cases} J - 1 & \text{in } \Omega^s, \\ \operatorname{Div}(J\boldsymbol{v}\boldsymbol{F}^{-T}) & \text{in } \Omega^f, \end{cases} \tag{56}$$

and the boundary conditions

$$\boldsymbol{\sigma}^f \boldsymbol{n} = \boldsymbol{\sigma}^s \boldsymbol{n} \quad \text{on } \Gamma_t^0, \qquad \boldsymbol{v} = \boldsymbol{v}_B \quad \text{on } \Gamma_t^1, \tag{57}$$

$$\boldsymbol{u} = \boldsymbol{0} \quad \text{on } \Gamma_t^2, \qquad \boldsymbol{\sigma}^f \boldsymbol{n} = \boldsymbol{0} \quad \text{on } \Gamma_t^3. \tag{58}$$

Let $I = [0, T]$ denote the time interval of interest. We multiply the equations (54)-(56) by the test functions $\boldsymbol{\zeta}, \boldsymbol{\xi}, \gamma$ such that $\boldsymbol{\zeta} = \boldsymbol{0}$ on Γ^2, $\boldsymbol{\xi} = \boldsymbol{0}$ on Γ^1 and integrate over the space domain Ω and the time interval I. Using integration by parts on some of the terms and the boundary conditions we obtain

$$\int_0^T \int_\Omega \frac{\partial \boldsymbol{u}}{\partial t} \cdot \boldsymbol{\zeta} dV dt = \int_0^T \int_{\Omega^s} \boldsymbol{v} \cdot \boldsymbol{\zeta} dV dt - \int_0^T \int_{\Omega^f} \operatorname{Grad} \boldsymbol{u} \cdot \operatorname{Grad} \boldsymbol{\zeta} dV dt, \tag{59}$$

$$\begin{aligned} \int_0^T \int_{\Omega^f} J\frac{\partial \boldsymbol{v}}{\partial t} \cdot \boldsymbol{\xi} dV dt + \int_0^T \int_{\Omega^s} \beta J \frac{\partial \boldsymbol{v}}{\partial t} \cdot \boldsymbol{\xi} dV dt & \\ = -\int_0^T \int_{\Omega^f} J \operatorname{Grad} \boldsymbol{v}\boldsymbol{F}^{-1}(\boldsymbol{v} - \frac{\partial \boldsymbol{u}}{\partial t}) \cdot \boldsymbol{\xi} dV dt & \\ + \int_0^T \int_\Omega Jp\boldsymbol{F}^{-T} \cdot \operatorname{Grad} \boldsymbol{\xi} dV dt & \\ - \int_0^T \int_{\Omega^s} \frac{\partial \Psi}{\partial \boldsymbol{F}} \cdot \operatorname{Grad} \boldsymbol{\xi} dV dt & \\ - \int_0^T \int_{\Omega^f} J\mu \operatorname{Grad} \boldsymbol{v}\boldsymbol{F}^{-1}\boldsymbol{F}^{-T} \cdot \operatorname{Grad} \boldsymbol{\xi} dV dt, & \end{aligned} \tag{60}$$

$$0 = \int_0^T \int_{\Omega^s} (J - 1)\gamma dV dt + \int_0^T \int_{\Omega^f} \operatorname{Div}(J\boldsymbol{v}\boldsymbol{F}^{-T})\gamma dV dt. \tag{61}$$

Let us define the following spaces

$$U = \{\boldsymbol{u} \in L^\infty(I, [W^{1,2}(\Omega)]^3), \boldsymbol{u} = \boldsymbol{0} \text{ on } \Gamma^2\},$$
$$V = \{\boldsymbol{v} \in L^2(I, [W^{1,2}(\Omega_t)]^3) \cap L^\infty(I, [L^2(\Omega_t)]^3), \boldsymbol{v} = \boldsymbol{0} \text{ on } \Gamma^1\},$$
$$P = \{p \in L^2(I, L^2(\Omega))\},$$

then the variational formulation of the fluid-structure interaction problem is to find $(\boldsymbol{u}, \boldsymbol{v} - \boldsymbol{v}_B, p) \in U \times V \times P$ such that equations (59), (60) and (61) are satisfied for all $(\boldsymbol{\zeta}, \boldsymbol{\xi}, \gamma) \in U \times V \times P$ including appropriate initial conditions.

3.4 Discretization

In the following, we restrict ourselves to two dimensions which allows systematic tests of the proposed methods in a very efficient way, particularly in view of grid-independent solutions. The time discretization is done by the Crank-Nicholson scheme which is only conditionally stable but which has better conservation properties than for example the implicit Euler scheme [see 6, 9]. The Crank-Nicholson scheme can be obtained by dividing the time interval I into the series of time steps $[t^n, t^{n+1}]$ with step length $k_n = t^{n+1} - t^n$. Assuming that the test functions are piecewise constant on each time step $[t^n, t^{n+1}]$, writing the weak formulation (59)-(60) for the time interval $[t^n, t^{n+1}]$, approximating the time derivatives by the central differences

$$\frac{\partial f}{\partial t} \approx \frac{f(t^{n+1}) - f(t^n)}{k_n} \tag{62}$$

and approximating the time integration for the remaining terms by the trapezoidal quadrature rule as

$$\int_{t^n}^{t^{n+1}} f(t)dt \approx \frac{k_n}{2}(f(t^n) + f(t^{n+1})), \tag{63}$$

we obtain the time discretized system. The last equation corresponding to the incompressibility constraint is taken implicitly for the time t^{n+1} and the corresponding term with the Lagrange multiplier p_h^{n+1} in the equation (60) is also taken implicitly.

The discretization in space is done by the finite element method. We approximate the domain Ω by a domain Ω_h with polygonal boundary and by $\mathcal{T}_h$ we denote a set of quadrilaterals covering the domain Ω_h. We assume that $\mathcal{T}_h$ is regular in the sense that any two quadrilateral are disjoint or have a common vertex or a common edge. By $\bar{T} = [-1, 1]^2$ we denote the reference quadrilateral.

Our treatment of the problem as one system suggests that we use the same finite elements on both, the solid part and the fluid region. Since both materials are incompressible we have to choose a pair of finite element spaces known to be stable for the problems with incompressibility constraint. One

possible choice is the conforming biquadratic, discontinuous linear Q_2, P_1 pair, see figure 3 for the location of the degrees of freedom. This choice results in 39 degrees of freedom per element in the case of our displacement, velocity, pressure formulation in two dimensions and 112 degrees of freedom per element in three dimensions.

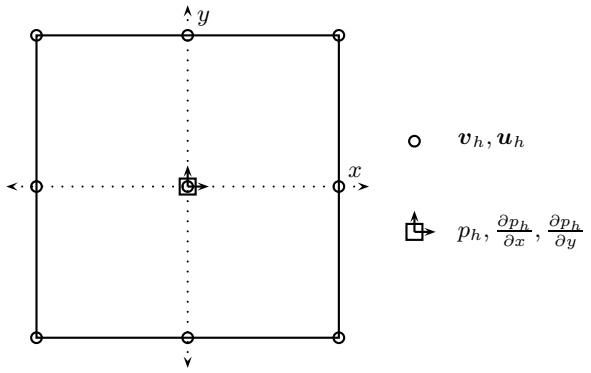

Fig. 3. Location of the degrees of freedom for the Q_2, P_1 element.

The spaces U, V, P on an interval $[t^n, t^{n+1}]$ would be approximated in the case of the Q_2, P_1 pair as

$$\begin{aligned}
U_h &= \{\boldsymbol{u}_h \in [C(\Omega_h)]^2, \boldsymbol{u}_h|_T \in [Q_2(T)]^2 \quad \forall T \in \mathcal{T}_h, \boldsymbol{u}_h = \boldsymbol{0} \text{ on } \Gamma_2\},\\
V_h &= \{\boldsymbol{v}_h \in [C(\Omega_h)]^2, \boldsymbol{v}_h|_T \in [Q_2(T)]^2 \quad \forall T \in \mathcal{T}_h, \boldsymbol{v}_h = 0 \text{ on } \Gamma_1\},\\
P_h &= \{p_h \in L^2(\Omega_h), p_h|_T \in P_1(T) \quad \forall T \in \mathcal{T}_h\}.
\end{aligned}$$

Let us denote by $\boldsymbol{u}_h^n$ the approximation of $\boldsymbol{u}(t^n)$, $\boldsymbol{v}_h^n$ the approximation of $\boldsymbol{v}(t^n)$ and p_h^n the approximation of $p(t^n)$. Further we will use following shorthand notation

$$\boldsymbol{F}^n = \boldsymbol{I} + \operatorname{Grad} \boldsymbol{u}_h^n, \quad J^n = \det \boldsymbol{F}^n \quad J^{n+\frac{1}{2}} = \frac{1}{2}(J^n + J^{n+1}),$$
$$(f,g) = \int_\Omega f \cdot g dV, \quad (f,g)_s = \int_{\Omega^s} f \cdot g dV, \quad (f,g)_f = \int_{\Omega^f} f \cdot g dV,$$

f, g being scalars, vectors or tensors.

Writing down the discrete equivalent of the equations (59)-(61) yields

$$\begin{aligned}
\left(\boldsymbol{u}_h^{n+1}, \boldsymbol{\eta}\right) - \frac{k_n}{2}\left\{ \left(\boldsymbol{v}_h^{n+1}, \boldsymbol{\eta}\right)_s + \left(\nabla \boldsymbol{u}_h^{n+1}, \nabla \boldsymbol{\eta}\right)_f \right\} \\
- \left(\boldsymbol{u}_h^{n}, \boldsymbol{\eta}\right) - \frac{k_n}{2}\left\{ \left(\boldsymbol{v}_h^{n}, \boldsymbol{\eta}\right)_s + \left(\nabla \boldsymbol{u}_h^{n}, \nabla \boldsymbol{\eta}\right)_f \right\} = 0,
\end{aligned} \tag{64}$$

$$
\begin{aligned}
&\left(J^{n+\frac{1}{2}}\boldsymbol{v}_h^{n+1},\boldsymbol{\xi}\right)_f + \beta\left(\boldsymbol{v}_h^{n+1},\boldsymbol{\xi}\right)_s - k_n\left(J^{n+1}p_h^{n+1}(\boldsymbol{F}^{n+1})^{-T},\operatorname{Grad}\boldsymbol{\xi}\right)_s \\
&\qquad + \frac{k_n}{2}\Bigg\{\left(\frac{\partial\Psi}{\partial\boldsymbol{F}}(\operatorname{Grad}\boldsymbol{u}_h^{n+1}),\operatorname{Grad}\boldsymbol{\xi}\right)_s \\
&\qquad + \mu\left(J^{n+1}\operatorname{Grad}\boldsymbol{v}_h^{n+1}(\boldsymbol{F}^{n+1})^{-1},\operatorname{Grad}\boldsymbol{\xi}(\boldsymbol{F}^{n+1})^{-1}\right)_f \\
&\qquad + \left(J^{n+1}\operatorname{Grad}\boldsymbol{v}_h^{n+1}(\boldsymbol{F}^{n+1})^{-1}\boldsymbol{v}_h^{n+1},\boldsymbol{\xi}\right)_f\Bigg\} \\
&\qquad - \frac{1}{2}\left(J^{n+1}\operatorname{Grad}\boldsymbol{v}_h^{n+1}(\boldsymbol{F}^{n+1})^{-1}(\boldsymbol{u}_h^{n+1}-\boldsymbol{u}_h^{n}),\boldsymbol{\xi}\right)_f \\
&\qquad - \left(J^{n+\frac{1}{2}}\boldsymbol{v}_h^{n},\boldsymbol{\xi}\right)_f - \beta\left(\boldsymbol{v}_h^{n},\boldsymbol{\xi}\right)_s \\
&\qquad + \frac{k_n}{2}\Bigg\{\left(\frac{\partial\Psi}{\partial\boldsymbol{F}}(\operatorname{Grad}\boldsymbol{u}_h^{n}),\operatorname{Grad}\boldsymbol{\xi}\right)_s \\
&\qquad + \mu\left(J^{n}\operatorname{Grad}\boldsymbol{v}_h^{n}(\boldsymbol{F}^{n})^{-1},\operatorname{Grad}\boldsymbol{\xi}(\boldsymbol{F}^{n})^{-1}\right)_f \\
&\qquad + \left(J^{n}\operatorname{Grad}\boldsymbol{v}_h^{n}(\boldsymbol{F}^{n})^{-1}\boldsymbol{v}_h^{n},\boldsymbol{\xi}\right)_f\Bigg\} \\
&\qquad + \frac{1}{2}\left(J^{n}\operatorname{Grad}\boldsymbol{v}_h^{n}(\boldsymbol{F}^{n})^{-1}(\boldsymbol{u}_h^{n+1}-\boldsymbol{u}_h^{n}),\boldsymbol{\xi}\right)_f = 0,
\end{aligned}
\tag{65}
$$

$$
\left(J^{n+1}-1,\gamma\right)_s + \left(J^{n+1}\operatorname{Grad}\boldsymbol{v}_h^{n+1}(\boldsymbol{F}^{n+1})^{-1},\gamma\right)_f = 0. \tag{66}
$$

Using the basis of the spaces U_h, V_h, P_h as the test functions $\boldsymbol{\zeta}, \boldsymbol{\xi}, \gamma$ we obtain a nonlinear algebraic set of equations. In each time step we have to find $\boldsymbol{X} = (\boldsymbol{u}_h^{n+1}, \boldsymbol{v}_h^{n+1}, p_h^{n+1}) \in U_h \times V_h \times P_h$ such that

$$
\boldsymbol{\mathcal{F}}(\boldsymbol{X}) = \boldsymbol{0}, \tag{67}
$$

where $\boldsymbol{\mathcal{F}}$ represents the system (64–66).

3.5 Solution algorithm

The system (67) of nonlinear algebraic equations is solved using Newton method as the basic iteration. One step of the Newton iteration can be written as

$$
\boldsymbol{X}^{n+1} = \boldsymbol{X}^{n} - \left[\frac{\partial\boldsymbol{\mathcal{F}}}{\partial\boldsymbol{X}}(\boldsymbol{X}^{n})\right]^{-1}\boldsymbol{\mathcal{F}}(\boldsymbol{X}^{n}). \tag{68}
$$

This basic iteration can exhibit quadratic convergence provided that the initial guess is sufficiently close to the solution. To ensure the convergence globally, some improvements of this basic iteration are used.

The damped Newton method with line search improves the chance of convergence by adaptively changing the length of the correction vector. The solution update step in the Newton method (68) is replaced by

$$
\boldsymbol{X}^{n+1} = \boldsymbol{X}^{n} + \omega\delta\boldsymbol{X}, \tag{69}
$$

where the parameter ω is determined such that a certain error measure decreases. One of the possible choices for the quantity to decrease is

$$f(\omega) = \boldsymbol{\mathcal{F}}(\boldsymbol{X}^n + \omega\delta\boldsymbol{X}) \cdot \delta\boldsymbol{X}. \tag{70}$$

Since we know

$$f(0) = \boldsymbol{\mathcal{F}}(\boldsymbol{X}^n) \cdot \delta\boldsymbol{X}, \tag{71}$$

and

$$f'(0) = \left[\frac{\partial \boldsymbol{\mathcal{F}}}{\partial \boldsymbol{X}}(\boldsymbol{X}^n)\right] \delta\boldsymbol{X} \cdot \delta\boldsymbol{X} = \boldsymbol{\mathcal{F}}(\boldsymbol{X}^n) \cdot \delta\boldsymbol{X}, \tag{72}$$

and computing $f(\omega_0)$ for $\omega_0 = -1$ or ω_0 determined adaptively from previous iterations, we can approximate $f(\omega)$ by a quadratic function

$$f(\omega) = \frac{f(\omega_0) - f(0)(\omega_0 + 1)}{\omega_0^2}\omega^2 + f(0)(\omega + 1). \tag{73}$$

Then setting

$$\tilde{\omega} = \frac{f(0)\omega_0^2}{f(\omega_0) - f(0)(\omega_0 + 1)}, \tag{74}$$

the new optimal step length $\omega \in [-1, 0]$ is

$$\omega = \begin{cases} -\dfrac{\tilde{\omega}}{2} & \text{if } \dfrac{f(0)}{f(\omega_0)} > 0, \\ -\dfrac{\tilde{\omega}}{2} - \sqrt{\dfrac{\tilde{\omega}^2}{4} - \tilde{\omega}} & \text{if } \dfrac{f(0)}{f(\omega_0)} \leq 0. \end{cases} \tag{75}$$

This line search can be repeated with ω_0 taken as the last ω until, for example, $f(\omega) \leq \frac{1}{2}f(0)$. By this we can enforce a monotone convergence of the approximation $\boldsymbol{X}^n$.

1. Let $\boldsymbol{X}^n$ be some starting guess.
2. Set the residuum vector $\boldsymbol{R}^n = \boldsymbol{\mathcal{F}}(\boldsymbol{X}^n)$ and the tangent matrix $\boldsymbol{A} = \frac{\partial \boldsymbol{\mathcal{F}}}{\partial \boldsymbol{X}}(\boldsymbol{X}^n)$.
3. Solve for the correction $\delta\boldsymbol{X}$
$$\boldsymbol{A}\delta\boldsymbol{X} = \boldsymbol{R}^n.$$
4. Find optimal step length ω.
5. Update the solution $\boldsymbol{X}^{n+1} = \boldsymbol{X}^n - \omega\delta\boldsymbol{X}$.

Fig. 4. One step of the Newton method with the line search.

An adaptive time-step selection was found to help in the nonlinear convergence. A heuristic algorithm was used to correct the time-step length

according to the convergence of the nonlinear iterations in the previous time-step. If the convergence was close to quadratic, i.e. only up to three Newton steps were needed to obtain the required precision, the time step could be slightly increased, otherwise the time-step length was reduced.

The structure of the Jacobian matrix $\frac{\partial \boldsymbol{\mathcal{F}}}{\partial \boldsymbol{X}}$ is

$$\frac{\partial \boldsymbol{\mathcal{F}}}{\partial \boldsymbol{X}}(\boldsymbol{X}) = \begin{pmatrix} S_{uu} & S_{uv} & 0 \\ S_{vu} & S_{vv} & B_u + B_v \\ B_u^T & B_v^T & 0 \end{pmatrix}, \tag{76}$$

and it can be computed by finite differences from the residual vector $\boldsymbol{\mathcal{F}}(\boldsymbol{X})$

$$\left[\frac{\partial \boldsymbol{\mathcal{F}}}{\partial \boldsymbol{X}}\right]_{ij} (\boldsymbol{X}^n) \approx \frac{[\boldsymbol{\mathcal{F}}]_i(\boldsymbol{X}^n + \alpha_j \boldsymbol{e}_j) - [\boldsymbol{\mathcal{F}}]_i(\boldsymbol{X}^n - \alpha_j \boldsymbol{e}_j)}{2\alpha_j}, \tag{77}$$

where $\boldsymbol{e}_j$ are the unit basis vectors in $\mathbb{R}^n$ and the coefficients α_j are adaptively taken according to the change in the solution in the previous time step. Since

α/TOL	10^{-8}	10^{-4}	10^{-2}	10^{-1}
10^{-8}	7 /107 [21.52]	12 /57 [26.52]	12 /47 [23.75]	17 /33 [27.38]
10^{-4}	7 /108 [24.57]	**8 /62 [17.77]**	**10 /42 [18.95]**	18 /31 [29.05]
10^{-2}	16 /109 [51.65]	20 /47 [38.28]	25 /29 [38.58]	56 /16 [73.83]
10^{-1}	44 /116 [141.30]	48 /35 [81.72]	49 /17 [65.77]	–

Table 1. nonlinear solver it. / avg. linear solver it. [CPU time] for BiCGStab(ILU(0)): TOL denotes the stopping criterion of the linear problems.

we know the sparsity pattern of the Jacobian matrix in advance, it is given by the used finite element method, this computation can be done in an efficient way so that the linear solver remains the dominant part in terms of the CPU time. However, as table 1 shows, the resulting nonlinear and linear solution behavior is quite sensitive w.r.t. the parameters.

3.6 Multigrid solver

The solution of the linear problems is the most time consuming part of the solution process. A good candidate seems to be a direct solver for sparse systems like UMFPACK [see 5]; while this choice provides very robust linear solvers, its memory and CPU time requirements are too high for larger systems (i.e. more than 20000 unknowns). Large linear problems can be solved by Krylov space methods (BiCGStab, GMRes [see 1]) with suitable preconditioners. One possibility is the ILU preconditioner with special treatment of the saddle point character of our system, where we allow certain fill-in for the zero diagonal blocks [see 2]. The alternative option for larger systems is the multigrid method presented in this section.

We utilize the standard geometric multigrid approach based on a hierarchy of grids obtained by successive regular refinement of a given coarse mesh. The complete multigrid iteration is performed in the standard defect-correction setup with the V or F-type cycle. While a direct sparse solver [5] is used for the coarse grid solution, on finer levels a fixed number (2 or 4) of iterations by local MPSC schemes (Vanka-like smoother) [23, 21] is performed. Such iteration can be written as

$$\begin{bmatrix} \boldsymbol{u}^{l+1} \\ \boldsymbol{v}^{l+1} \\ p^{l+1} \end{bmatrix} = \begin{bmatrix} \boldsymbol{u}^{l} \\ \boldsymbol{v}^{l} \\ p^{l} \end{bmatrix} - \omega \sum_{\text{Patch } \Omega_i} \begin{bmatrix} S_{\boldsymbol{uu}|\Omega_i} & S_{\boldsymbol{uv}|\Omega_i} & 0 \\ S_{\boldsymbol{vu}|\Omega_i} & S_{\boldsymbol{vv}|\Omega_i} & kB_{|\Omega_i} \\ c_{\boldsymbol{u}} B^T_{s|\Omega_i} & c_{\boldsymbol{v}} B^T_{f|\Omega_i} & 0 \end{bmatrix}^{-1} \begin{bmatrix} \mathbf{def}^l_{\boldsymbol{u}} \\ \mathbf{def}^l_{\boldsymbol{v}} \\ def^l_p \end{bmatrix}.$$

The inverse of the local systems (39×39) can be done by hardware optimized direct solvers.

The full nodal interpolation is used as the prolongation operator $\boldsymbol{P}$ with its transposed operator used as the restriction $\boldsymbol{R} = \boldsymbol{P}^T$.

In table 2 we compare the performance of the multigrid solver with the Krylov space based iterative solvers with ILU preconditioner. The comparison

timestep 10^{-2}

Level	ndof	MG(2)	MG(4)	BiCGStab(ILU(1))	GMRES(ILU(1),200)
1	12760	2/8 [66]	2/8 [92]	2/51 [32]	2/50 [27]
2	50144	2/8 [190]	2/5 [198]	2/120 [200]	2/117 [151]
3	198784	2/9 [744]	2/6 [852]	2/311 [1646]	2/358 [1432]
4	791552	2/13 [3803]	2/7 [3924]	MEM.	MEM.

timestep 10^{0}

Level	ndof	MG(2)	MG(4)	BiCGStab(ILU(1))	GMRES(ILU(1),200)
1	12760	4/12 [118]	4/11 [177]	20/160 [631]	20/801 [1579]
2	50144	4/12 [466]	4/7 [470]	2/800 [] diverg.	13/801 [] diverg.
3	198784	4/13 [1898]	4/7 [2057]	2/800 [] diverg.	4/801 [] diverg.
4	791552	4/15 [8678]	4/8 [9069]	MEM.	MEM.

Table 2. Comparison of different solvers (nonlinear solver it. / avg. linear solver it. [CPU time]).

is presented for two different sizes of the timestep to illustrate the behavior of the solvers for different level of nonlinearity involved.

4 Examplary applications in biomechanics

In this section we present a few example applications to demonstrate the described methods. As a motivation we consider the numerical simulation of some problems encountered in the area of cardiovascular hemodynamics, namely flow interaction with thick-walled deformable material, which can

become a useful tool for deeper understanding of the onset of diseases of the human circulatory system, as for example blood cell and intima damages in stenosis, aneurysm rupture, evaluation of the new surgery techniques of heart, arteries and veins.

In order to test the proposed numerical methods, simplified two-dimensional examples which include interaction of flow with deformable material are computed. The first example is a flow in an ellipsoidal cavity and the second is a flow through a channel with elastic walls. In both cases the flow is driven by changing the fluid pressure at the inflow part of the boundary while the elastic part of the boundary is either fixed or stress free.

The constitutive relations used for the materials are the incompressible Newtonian model (49) for the fluid and the hyper-elastic neo-Hookean material (53) with $c_2 = 0$ for the solid. This choice includes all the main difficulties the numerical method has to deal with, namely the incompressibility and significant deformations.

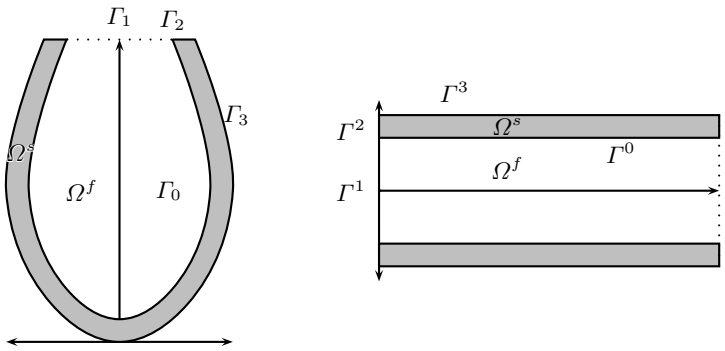

Fig. 5. Schematic view of the ventricle and elastic tube geometries.

4.1 Flow in an ellipsoidal cavity

The motivation for our first test is the left heart ventricle which is an approximately ellipsoidal chamber surrounded by the heart muscle. In our two-dimensional computations we use an ellipsoidal cavity, see figure 5, with prescribed time-dependent natural boundary condition at the fluid boundary part Γ^1

$$p(t) = \sin t \quad \text{on } \Gamma^1. \tag{78}$$

The material of the solid wall is modelled by the simple neo-Hookean constitutive relation (53) with $c_2 = 0$.

The figures 6 and 7 show the computational grid for the maximal and minimal volume configuration of the cavity and the velocity field of the fluid

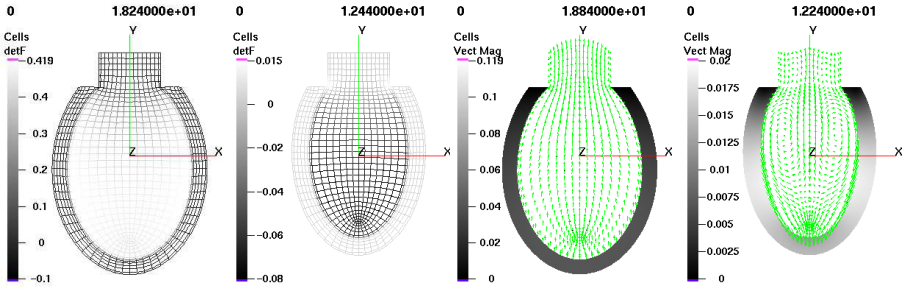

Fig. 6. Maximum and minimum volume configuration with the fluid flow.

for the same configurations. One of the important characteristics is the shear stress exerted by the fluid flow on the wall material. This figure 7 shows the distribution of the shear stress in the domain for three different times. In

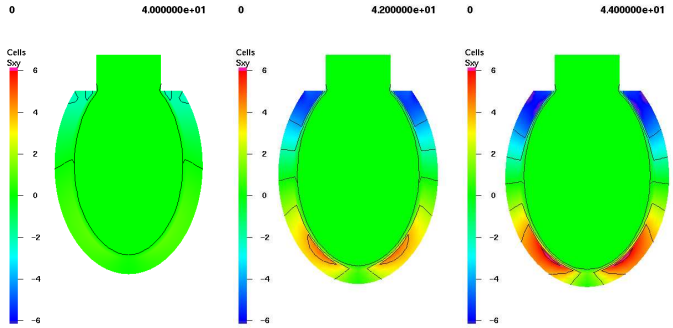

Fig. 7. Shear stress distribution in the wall during the period.

figures 8 and 9 the volume change of the cavity as a function of the time and the average pressure inside the cavity vs. the volume of the cavity is shown together with the trajectory and velocity of a material point on the solid-fluid interface. We can see that after the initial cycle which was started from the undeformed configuration the system comes to a time periodic solution.

4.2 Flow in an elastic channel

The second application is the simulation of a flow in an elastic tube or in our 2 dimensional case a flow between elastic plates. The flow is driven by a time-dependent pressure difference between the ends of the channel of the form (78). Such flow is also interesting to investigate in the presence of some constriction as a stenosis, which is shown in figure 13.

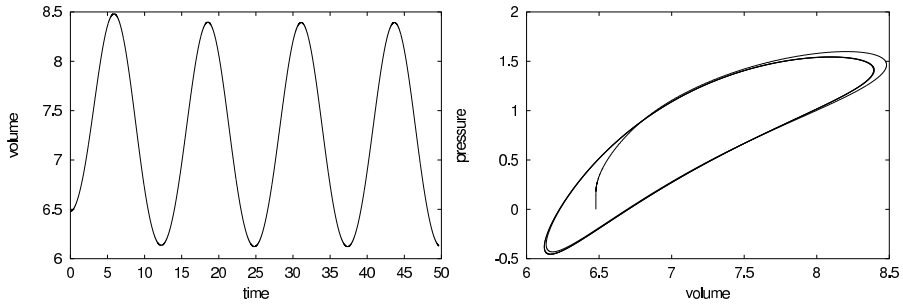

Fig. 8. Volume of the fluid inside and the pressure-volume diagram for the ellipsoidal cavity test.

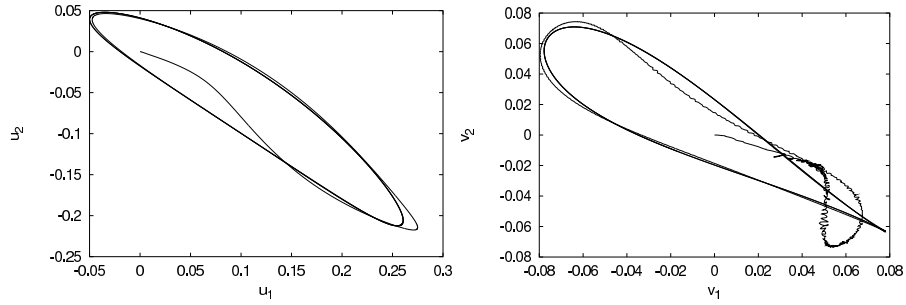

Fig. 9. The displacement trajectory and velocity of a point at the fluid-solid interface (inner side of the wall) for the ellipsoidal cavity test.

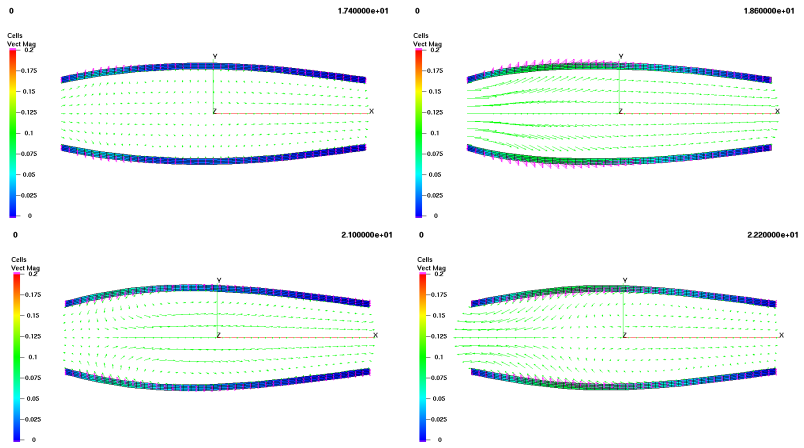

Fig. 10. Velocity field during one pulse in a channel without an obstacle.

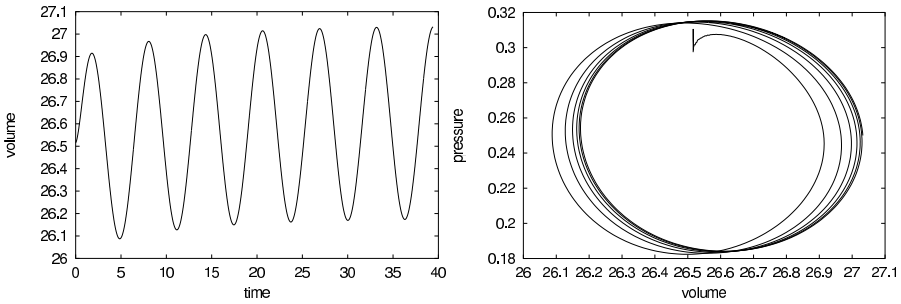

Fig. 11. Volume of the fluid in the channel and the pressure-volume diagram.

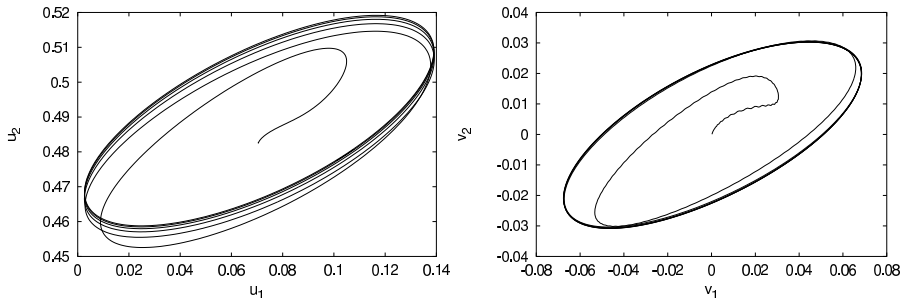

Fig. 12. Displacement trajectory and velocity of a point at the fluid solid interface (inner side of the wall).

For the flow in the channel without any constriction the time dependence of the fluid volume inside the channel is shown together with the pressure volume diagram in the figure and the trajectory and velocity of a material point on the solid fluid interface in the figures 11 and 12. The velocity field is shown in figure 10 at different stages of the pulse.

Finally in figure 13 the velocity field in the fluid and the pressure distribution throughout the wall is shown for the computation of the flow in a channel with elastic obstruction. In this example the elastic obstruction is modelled by the same material as the walls of the channel and is fixed to the elastic walls. Both ends of the walls are fixed at the inflow and outflow and the flow is again driven by a periodic change of the pressure at the left end.

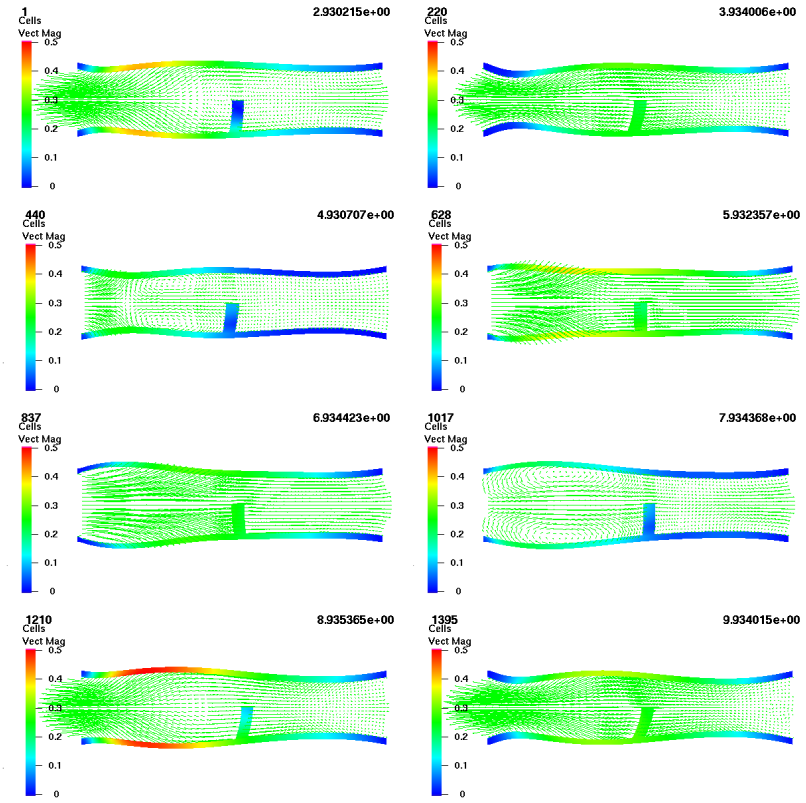

Fig. 13. Fluid flow and pressure distribution in the wall during one pulse for the example flow in a channel with constriction.

5 Summary and future development

In this paper we presented a general formulation of dynamic fluid-structure interaction problem suitable for applications with finite deformations and laminar flows. While the presented example calculations are simplified to allow initial testing of the numerical methods [see 22] the formulation is general enough to allow immediate extension to more realistic material models. For example in the case of material anisotropy one can consider

$$\tilde{\Psi} = c_1(I_C - 3) + c_2(II_C - 3) + c_3(|\boldsymbol{F}\boldsymbol{a}| - 1)^2,$$

with $\boldsymbol{a}$ being the preferred material direction. The term $|\boldsymbol{F}\boldsymbol{a}|$ represents the extension in the direction $\boldsymbol{a}$. The system can be coupled with additional models of chemical and electric activation of the active response of the biological material [see 11]. In the same manner the constitutive relation for the fluid can be directly extended to the power law models used to describe the shear thinning property of blood. Further extension to viscoelastic models and coupling with the mixture based model for soft tissues together with models for chemical and electric processes involved in biomechanical problems would allow to perform realistic simulation for real applications.

To obtain the solution approximation the discrete systems resulting from the finite element discretization of the governing equations need to be solved which requires sophisticated solvers of nonlinear systems and fast solvers for very large linear systems. The computational complexity increases tremendously for full 3D problems and with more complicated models like viscoelastic materials for the fluid or solid components. The main advantage of the presented numerical method is its accuracy and robustness with respect to the constitutive models. Possible directions of increasing the efficiency of the solvers include the development of improved multigrid solvers, for instance of global pressure Schur complement type [21], and the combination with parallel high performance computing techniques.

Bibliography

[1] R. Barrett, M. Berry, T. F. Chan, J. Demmel, J. Donato, J. Dongarra, V. Eijkhout, R. Pozo, C. Romine, and H. Van der Vorst. *Templates for the solution of linear systems: Building blocks for iterative methods*. SIAM, Philadelphia, PA, second edition, 1994.

[2] R. Bramley and X. Wang. *SPLIB: A library of iterative methods for sparse linear systems*. Department of Computer Science, Indiana University, Bloomington, IN, 1997. `http://www.cs.indiana.edu/ftp/bramley/splib.tar.gz`.

[3] K. D. Costa, P. J. Hunter, Rogers J. M., J. M. Guccione, L. K. Waldman, and A. D. McCulloch. A three-dimensional finite element method for large elastic deformations of ventricular myocardum: I – Cylindrical and spherical polar coordinates. *Trans. ASME J. Biomech. Eng.*, 118(4):452–463, 1996.

[4] K. D. Costa, P. J. Hunter, J. S. Wayne, L. K. Waldman, J. M. Guccione, and A. D. McCulloch. A three-dimensional finite element method for large elastic deformations of ventricular myocardum: II – Prolate spheroidal coordinates. *Trans. ASME J. Biomech. Eng.*, 118(4):464–472, 1996.

[5] T. A. Davis and I. S. Duff. A combined unifrontal/multifrontal method for unsymmetric sparse matrices. *ACM Trans. Math. Software*, 25(1):1–19, 1999.

[6] Charbel Farhat, Michel Lesoinne, and Nathan Maman. Mixed explicit/implicit time integration of coupled aeroelastic problems: three-field formulation, geometric conservation and distributed solution. *Int. J. Numer. Methods Fluids*, 21(10):807–835, 1995. Finite element methods in large-scale computational fluid dynamics (Tokyo, 1994).

[7] Matthias Heil. Stokes flow in collapsible tubes: Computation and experiment. *J. Fluid Mech.*, 353:285–312, 1997.

[8] Matthias Heil. Stokes flow in an elastic tube - a large-displacement fluid-structure interaction problem. *Int. J. Num. Meth. Fluids*, 28(2):243–265, 1998.

[9] Bruno Koobus and Charbel Farhat. Second-order time-accurate and geometrically conservative implicit schemes for flow computations on unstructured dynamic meshes. *Comput. Methods Appl. Mech. Engrg.*, 170(1-2):103–129, 1999.

[10] Patrick Le Tallec and Salouna Mani. Numerical analysis of a linearised fluid-structure interaction problem. *Num. Math.*, 87(2):317–354, 2000.

[11] W. Maurel, Y. Wu, N. Magnenat Thalmann, and D. Thalmann. *Biomechanical models for soft tissue simulation*. ESPRIT basic research series. Springer-Verlag, Berlin, 1998.

[12] K. D. Paulsen, M. I. Miga, F. E. Kennedy, P. J. Hoopes, A. Hartov, and D. W. Roberts. A computational model for tracking subsurface tissue deformation during stereotactic neurosurgery. *IEEE Transactions on Biomedical Engineering*, 46(2):213–225, 1999.

[13] Charles S. Peskin. Numerical analysis of blood flow in the heart. *J. Computational Phys.*, 25(3):220–252, 1977.

[14] Charles S. Peskin. The fluid dynamics of heart valves: experimental, theoretical, and computational methods. In *Annual review of fluid mechanics, Vol. 14*, pages 235–259. Annual Reviews, Palo Alto, Calif., 1982.

[15] Charles S. Peskin and David M. McQueen. Modeling prosthetic heart valves for numerical analysis of blood flow in the heart. *J. Comput. Phys.*, 37(1):113–132, 1980.

[16] Charles S. Peskin and David M. McQueen. A three-dimensional computational method for blood flow in the heart. I. Immersed elastic fibers in a viscous incompressible fluid. *J. Comput. Phys.*, 81(2):372–405, 1989.

[17] A. Quarteroni. Modeling the cardiovascular system: a mathematical challenge. In B. Engquist and W. Schmid, editors, *Mathematics Unlimited - 2001 and Beyond*, pages 961–972. Springer-Verlag, 2001.

[18] A. Quarteroni, M. Tuveri, and A. Veneziani. Computational vascular fluid dynamics: Problems, models and methods. *Computing and Visualization in Science*, 2(4):163–197, 2000.

[19] M. Rumpf. On equilibria in the interaction of fluids and elastic solids. In *Theory of the Navier-Stokes equations*, pages 136–158. World Sci. Publishing, River Edge, NJ, 1998.

[20] P. A. Sackinger, P. R. Schunk, and R. R. Rao. A Newton-Raphson pseudo-solid domain mapping technique for free and moving boundary problems: a finite element implementation. *J. Comput. Phys.*, 125(1):83–103, 1996.

[21] S. Turek. *Efficient solvers for incompressible flow problems: An algorithmic and computational approach.* Springer, 1999.

[22] S. Turek and J. Hron. Proposal for numerical benchmarking of fluid-structure interaction between an elastic object and laminar incompressible flow. In H.-J. Bungartz and M. Schäfer, editors, *Fluid-Structure Interaction: Modelling, Simulation, Optimisation*, LNCSE. Springer, 2006.

[23] S.P. Vanka. Implicit multigrid solutions of Navier-Stokes equations in primitive variables. *J. of Comp. Phys.*, (65):138–158, 1985.